

DOI 10.24425/ae.2022.140722

Finite element analysis of mechanical stress in in-wheel motor

JIE XU  

Shandong University of Technology, School of Transportation and Vehicle Engineering
China

e-mail: 19402010032@stumail.sdut.edu.cn

(Received: 11.05.2021, revised: 13.01.2022)

Abstract: When the in-wheel motor is working, it will be affected by gravity, centrifugal force and electromagnetic force. These three kinds of mechanical loads will affect the mechanical stress characteristics of the in-wheel motor, and then affect the reliability of the in-wheel motor structure. In order to understand the influence of the above loads on the mechanical stress of the in-wheel motor, this paper takes a 15-kW built-in permanent magnet in-wheel motor as the research object. Based on the establishment of the electromagnetic field and structure field coupling analysis model of the in-wheel motor, the mechanical stress of the in-wheel motor under different mechanical loads under rated and peak conditions are calculated and analyzed, and the influence of different mechanical loads on the stress and deformation of the in-wheel motor are studied. The research results show that, regardless of the rated operating condition or the peak operating condition, the in-wheel motor has the largest mechanical stress and deformation under the combined action of centrifugal force and electromagnetic force, and the smallest mechanical stress and deformation under the action of gravity only; under the same load (except for the case of gravity only), the stress and deformation of the in-wheel motor under the peak operating condition are larger than those under the rated operating condition; and the maximum stress and deformation of the in-wheel motor appear at the rotor magnetic bridge and the inner edge of the rotor, respectively, so the rotor is an easily damaged part of the in-wheel motor.

Key words: deformation, in-wheel motor, mechanical loads, mechanical stress

1. Introduction

The in-wheel motor drive is a technology that integrates in-wheel motors, brakes, and deceleration mechanisms into the wheels [1], and electric vehicles driven by in-wheel motors are currently one of the development directions of automobiles [2–4]. When the in-wheel motor



© 2022. The Author(s). This is an open-access article distributed under the terms of the Creative Commons Attribution-NonCommercial-NoDerivatives License (CC BY-NC-ND 4.0, <https://creativecommons.org/licenses/by-nc-nd/4.0/>), which permits use, distribution, and reproduction in any medium, provided that the Article is properly cited, the use is non-commercial, and no modifications or adaptations are made.

drives the electric vehicle to work, the in-wheel motor is usually subjected to the load of gravity and centrifugal force. Based on the action of the two loads, the three-phase winding in the stator of the permanent magnet synchronous in-wheel motor generates a rotating magnetic field due to the passing of current. The magnetic field and the excitation magnetic field generated by the permanent magnet will interact, and the resulting electromagnetic force will also act on the in-wheel motor. These three kinds of mechanical loads act on the structure of the in-wheel motor, which will have a certain impact on the mechanical stress and deformation of the in-wheel motor. Therefore, the accurate analysis of mechanical stress is very important to the research on the reliability of the in-wheel motor structure.

For the mechanical stress characteristics in the structural field of the in-wheel motor, scholars at home and abroad have done certain research. Taking the built-in rotor core of permanent magnets as the research object, references [5, 6] studied the influence of centrifugal force on rotor mechanical stress by an analytical method, and obtained the influence law of different operating states and interference on rotor mechanical stress. Reference [7] took the permanent magnet synchronous motor as the research object, used Hooke's law to change the motor speed to study the influence of different centrifugal forces on the mechanical stress of the magnetic bridge. References [8–11] used finite element and analytical methods to study the mechanical stress of a variety of permanent magnet synchronous motors, only considered the impact of centrifugal force on the mechanical stress of the rotor, calculated the stress concentration factor, and determined the trend of the maximum mechanical stress on the rotor magnetic bridge with the change of geometric parameters. Reference [12] only considered the influence of centrifugal force on the built-in permanent magnet synchronous motors, used the finite element method to calculate the mechanical stress, and determined that the magnetic bridge is the weak area in the motor. Reference [13] used the virtual displacement method to calculate the electromagnetic force in the electromagnetic field, and then loaded the electromagnetic force to the structure field. The mechanical stress distribution at the winding end was obtained in accordance with the actual situation, and the position of the maximum stress at the winding end was determined. Reference [14] calculated the mechanical stress of the rotor under the action of electromagnetic force through the finite element method, and determined that the maximum stress of the rotor would decrease with the increase of the width of the magnetic bridge and the magnetic rib. Reference [15] used finite element and analytical methods to compare the stator deformation distribution with and without electromagnetic force, and concluded that the electromagnetic force has a significant effect on the stator deformation. Reference [16] used the finite element method to study the influence of electromagnetic force and centrifugal force on the rotor stress, and determined that the rotor would not generate friction with the stator part during operation. Both the obtained maximum rotor stress and maximum deformation met the mechanical strength requirements of the motor. Reference [17] took the rotor of a low-speed and high-torque permanent magnet synchronous motor as the research object, used the finite element method to analyze the deformation distribution of the rotor under the action of gravity, centrifugal force and electromagnetic force, optimized the structure to make the rotor deformation smaller, and found the influence law between rotor structure strength and structural parameters. To sum up, there have been certain studies on the mechanical stress of in-wheel motors at home and abroad, but most of the current researches only analyze the mechanical stress of the rotor, stator and other parts during the operation of the in-wheel mo-

tor, and mechanical loads are not considered comprehensively in the research, which leads to the unclear mechanism of the mechanical stress of the in-wheel motor. In fact, the in-wheel motor bears multiple loads such as gravity, centrifugal force and electromagnetic force at the same time during the operating process. Different loads have different effects on the stress and deformation of the motor, and further affect the reliability of the motor structure. Therefore, the calculation of the mechanical stress of the in-wheel motor under different mechanical loads is of great significance to the research on the structural reliability of the in-wheel motor.

Based on this, this paper takes a 15-kW built-in permanent magnet in-wheel motor as the research object. After establishing the electromagnetic field and structure field coupling model of the in-wheel motor, the mechanical stress characteristics of the in-wheel motor under different operating conditions and mechanical loads are systematically analyzed. Furthermore, the influence law of different mechanical loads on the stress and deformation of the in-wheel motor is obtained. The research results of this paper can lay a certain foundation for the subsequent reliability research of the in-wheel motor structure.

2. The structure of the in-wheel motor

The built-in permanent magnet in-wheel motor in this article has an inner rotor and outer stator structure. Figure 1 below shows the in-wheel motor structure. Table 1 shows the specific performance parameters of the in-wheel motor.

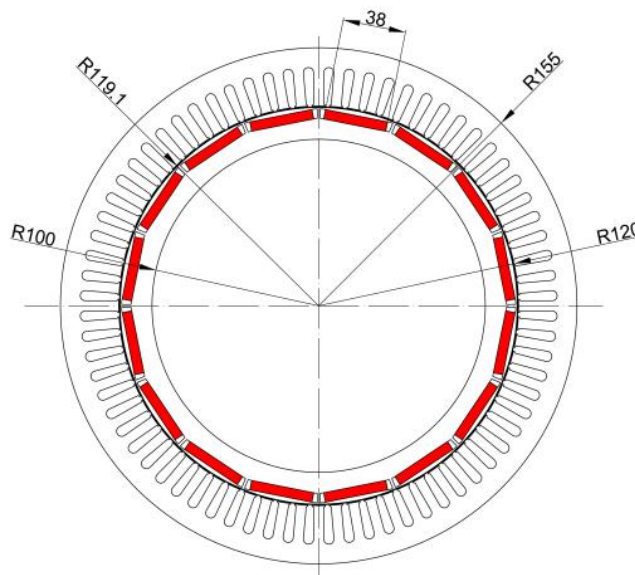


Fig. 1. Structure of in-wheel motor

Table 1. Basic performance parameters of in-wheel motor

Name	Value	Name	Value
Rated power	15 kW	Peak power	54 kW
Rated speed	1000 r/min	Peak speed	1100 r/min
Rated torque	143.25 N·m	Peak torque	468.82 N·m

3. Establishment of electromagnetic field and structure field coupling model of in-wheel motor

In this paper, research on the mechanical stress of the in-wheel motor involves the coupling of the electromagnetic field and structure field. Therefore, the finite element method is used to establish the electromagnetic field and structure field coupling model of the in-wheel motor [18], and the mechanical stress analysis of the in-wheel motor under different operating conditions and loads is carried out.

3.1. Basic assumptions

Before establishing the electromagnetic field and structure field coupling model, the following basic assumptions need to be made [19]:

1. Does not consider the influence of temperature;
2. In order to simplify the calculation of the finite element method, the mechanical stress analysis of the two-dimensional in-wheel motor is carried out, and the axial stress of the in-wheel motor is not counted;
3. The centrifugal effect at a constant speed is constant in time.

3.2. Determination of material properties

In the in-wheel motor, the material of the stator iron and rotor is DW465-50, the material of the permanent magnet is NdFeB 33UH, the material of the chassis is structural steel, and the material of the coil is copper. In addition, the specific parameters of the materials used in the key parts of the in-wheel motor are shown in Table 2.

3.3. Boundary conditions and loads of model

Since this research involves the coupling of the electromagnetic field and the structural field of the in-wheel motor, the boundary conditions and loads of the model include the electromagnetic part and structural part.

In the electromagnetic field of the in-wheel motor, the initial values of the two components of the vector magnetic potential and the scalar magnetic potential are all 0, and this initial value is used as the initial condition for solving the transient magnetic field. The normal component B_n of the magnetic flux density at the outermost boundary of the chassis is also 0 [20]. In the field of the in-wheel motor structure, first of all, in the setting of constraints, in order to realize that the stator and rotor bracket are stationary relative to the rotor, respectively, the boundary condition

Table 2. Material properties

Part	Material	Conductivity (S/m)	Relative permittivity	Density (kg/m ³)	Poisson's ratio	Elasticity modulus (MPa)	Allowable stress (MPa)
Stator iron/ Rotor	DW465-50	$2.63 \cdot 10^6$	1	7700	0.26	$1.96 \cdot 10^5$	92
Permanent magnets	NdFeB 33UH	$6.25 \cdot 10^5$	1	7800	0.23	$1.5 \cdot 10^5$	24
Coil	Copper	$6 \cdot 10^7$	1	8900	0.324	$1.1 \cdot 10^5$	72
Chassis	Structural steel	1	1	7850	0.3	$2 \cdot 10^5$	142
Insulation	Insulation materials	1	1	1300	0.34	$2.25 \cdot 10^5$	24

with fixed constrain is used for the area where the stator and rotor bracket are located, that is, to constrain its 2 degrees of freedom in the translation direction and 1 degree of freedom in the rotation direction. Then, in the setting of the contact, the stator and the insulating, the insulating and the coil, the rotor and the permanent magnets are all bonded and contacted by glue. There is an interference fit between the chassis and the stator, the rotor and the rotor bracket, the end cap and the support shaft. The boundary between the rotor bracket and the end cap in contact with each other can be connected in the normal direction and can slide freely in the tangential direction. Finally, in the load setting, add gravity to the in-wheel motor, add centrifugal force to the rotor, permanent magnets and other parts, and couple the electromagnetic force in the electromagnetic field to the structure field through the grid nodes.

3.4. Establishment of finite element model

According to the determined structure, basic assumptions, material properties, boundary conditions and loads, a finite element model of the in-wheel motor is established. In the finite element model, the types of finite elements used are plane magnetic field elements and plane stress elements, and the solver is a direct solver. In addition, for the grid division of the electromagnetic field model, the air gap is divided into two, and the air gap grid near the rotor side is more refined than the grid near the stator side. In the grid division of the structural field model, since the stress at the magnetic bridge is very susceptible to the influence of the grid density [21], the grid density at the magnetic bridge must be increased. Figure 2 shows the quarter finite element model in the structure field, including grids, partial loads and constraints.

3.5. Verification of the validity of the model

In order to ensure the validity of the structural field model, the grid independence is tested [22]. Since this paper calculates the mechanical stress of the in-wheel motor, the relative change rate of the average value of the in-wheel motor deformation is used as a reference for testing the

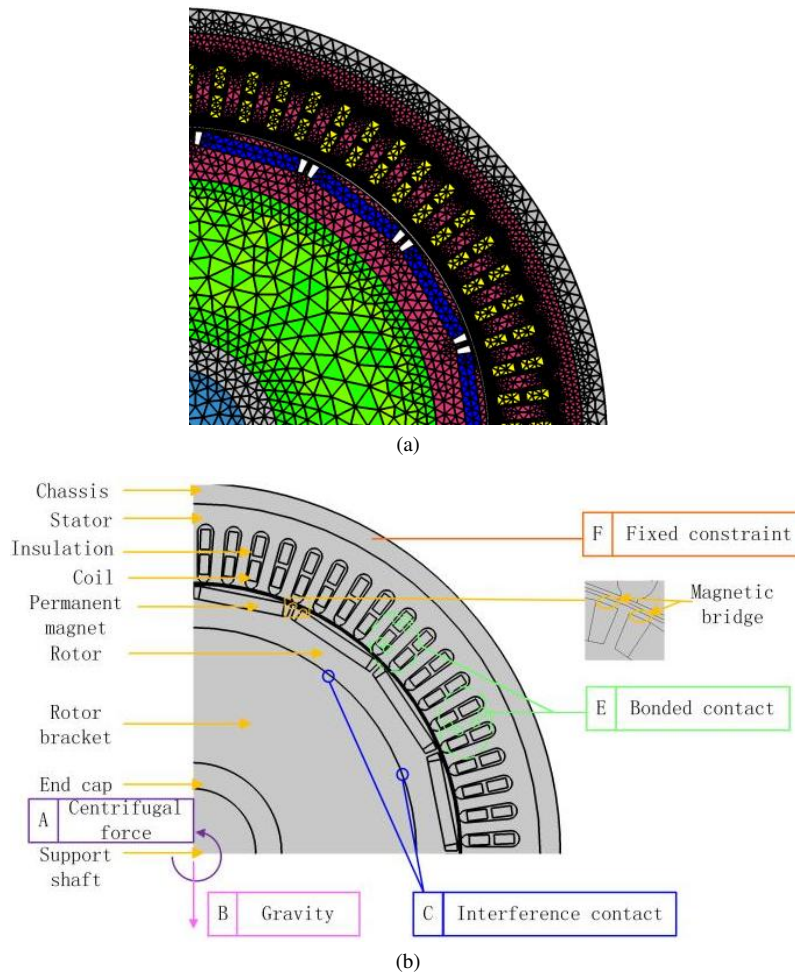


Fig. 2. 1/4 finite element model: (a) grids; (b) partial loads and constraints

independence of the grid. In this paper, it is assumed that when the relative change rate of the average deformation is less than 0.05%, the grid is independent. Next, if the average deformation of the finite element model of the in-wheel motor is d_m and d_n when the number of grids is m and n , then Eq. (1) can be used to calculate the relative change rate (η) of the average deformation of the in-wheel motor.

$$\eta = \frac{|d_m - d_n|}{d_m} \cdot 100\%, \quad (1)$$

where: η is the relative change rate of the average deformation, d_m and d_n are the average deformations when the grid is m and n , respectively.

Figure 3 shows the change of the relative change rate of the average value of the deformation of the in-wheel motor under the simultaneous action of gravity, centrifugal force and electromagnetic force with the number of grids. It can be seen from the figure that as the number of grids increases,

the relative change rate of the average deformation gradually stabilizes, and finally is less than 0.05%, which meets the requirements of grid independence. In addition, considering that the number of grids will also affect the calculation time of the model, finally, the number of grids in the structure field is determined to be 43 000.

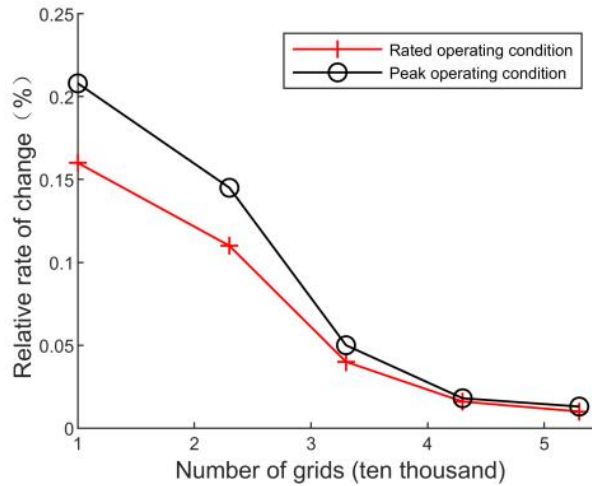


Fig. 3. Diagram of relative rate of change

After verifying the validity of the structural field model, it is also necessary to verify the validity of the electromagnetic field model. By comparing the motor torque calculated by the finite element method with the design torque, the relative error of the torque is obtained, as shown in Table 3. It can be seen from Table 3 that under the same operating condition, the relative error of the torque value is less than 5%. Therefore, the electromagnetic field model is effective.

Table 3. Torque and relative error

	Finite Element Method (N·m)	Design value (N·m)	Relative error (%)
Rated operating condition	146.02	143.25	1.93
Peak operating condition	487.62	468.82	4.01

4. Result analysis

After the electromagnetic field and structure field coupling model of the in-wheel motor is established, the mechanical stress of the in-wheel motor under the action of a single load, two loads and combination of 3 loads (gravity, centrifugal force and electromagnetic force) is calculated separately by the application of changed mechanical loads. In addition, the influence of different mechanical loads on the stress and deformation of the in-wheel motor are studied.

4.1. The influence of mechanical loads on the mechanical stress of in-wheel motor

Under the rated operating condition of the in-wheel motor, the mechanical stress distribution of the in-wheel motor under different loads is obtained by calculating the coupling model. When considering the influence of electromagnetic force on mechanical stress, the electromagnetic force at 0.06 s, when the electromagnetic field is in a stable state, is used as the load for the steady-state structural field analysis of the in-wheel motor. Since gravity acts uniformly on the in-wheel motor in the Cartesian coordinate system, and centrifugal force acts uniformly on the in-wheel motor in the cylindrical coordinate system. But the electromagnetic force acts on the motor unevenly in the Cartesian coordinate system. So, the mechanical stress (von Mises) distribution at 0.06 s under the action of gravity and centrifugal force, electromagnetic force only and the combination of three loads are shown in Fig. 4. It can be seen from Fig. 4 that under the influence of different loads,

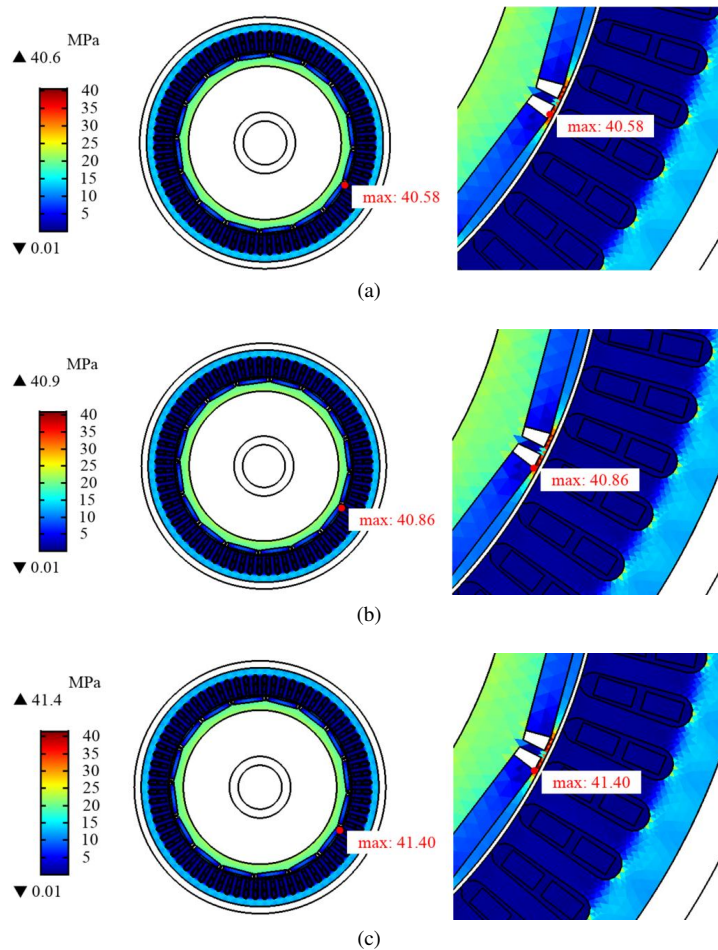


Fig. 4. Mechanical stress (von Mises) distribution under rated condition: (a) gravity and centrifugal force; (b) electromagnetic force only; (c) combination of 3 loads

the mechanical stress on the rotor is obviously greater than that on other parts. Moreover, the maximum mechanical stress of the in-wheel motor is in the magnetic bridge of the rotor, thus the rotor is an easily damaged part of the in-wheel motor. In addition, under the same load condition, comparing the mechanical stress distribution under the rated condition and peak condition, the law of mechanical stress distribution of the in-wheel motor under the peak condition is the same as that under the rated condition, and the only difference is that the mechanical stress values are different. In order to simplify the content of the article, the mechanical stress distribution under the peak condition is no longer displayed.

Table 4 shows the maximum mechanical stress of the in-wheel motor under different operating conditions and loads. Table 5 shows the average values of the mechanical stress of the in-wheel motor under different operating conditions and loads. It can be seen from Tables 4 and 5, that under the same operating condition, the influence of a single load on the maximum mechanical stress

Table 4. Maximum mechanical stress of in-wheel motor (MPa)

		Rated operating condition	Peak operating condition
Single load	Gravity only	40	40
	Centrifugal force only	40.59	40.71
	Electromagnetic force only	40.86	41.18
Two loads	Gravity and centrifugal force	40.58	40.70
	Gravity and electromagnetic force	40.85	40.17
	Centrifugal force and electromagnetic force	41.41	41.87
Three loads	Combination of 3 loads	41.40	41.86

Table 5. Average values of mechanical stress of in-wheel motor (MPa)

		Rated operating condition	Peak operating condition
Single load	Gravity only	7.68	7.68
	Centrifugal force only	7.74	7.75
	Electromagnetic force only	7.78	7.85
Two loads	Gravity and centrifugal force	7.74	7.75
	Gravity and electromagnetic force	7.78	7.85
	Centrifugal force and electromagnetic force	7.83	7.92
Three loads	Combination of 3 loads	7.83	7.92

and the average value of mechanical stress is sorted from small to large, in order of gravity only, centrifugal force only, and electromagnetic force only. This is because the greater the load, the greater the mechanical stress. Similarly, the influence of two loads on the maximum mechanical stress and the average value of mechanical stress is sorted from small to large, followed by gravity and centrifugal force, gravity and electromagnetic force, centrifugal force and electromagnetic force. However, due to the different loading directions, there is an offset effect. The maximum mechanical stress under the combined action of three loads is smaller than the value under the action of centrifugal force and electromagnetic force. After calculating the average stress value, the offset effect among three loads is weakened, so that the average stress under the combination of three loads is as large as that under the action of centrifugal force and electromagnetic force. On the other hand, under the same load (except for the case of gravity only), the maximum values and the average values of the mechanical stress of the in-wheel motor under the peak condition are greater than the corresponding values under the rated condition. This is because the electromagnetic force and centrifugal force under the peak condition are greater than the corresponding values under the rated condition, and the magnitude of the load affects the mechanical stress. The size of the centrifugal force is determined by the rotational speed of the in-wheel motor. Because the peak rotational speed is greater than the rated rotational speed, the centrifugal force of the rotor and permanent magnets under the peak condition is greater than the centrifugal force under the rated condition. In addition, the coil current excitation value under the peak operating condition is larger than the value under the rated operating condition, causing the rotating magnetic field under the peak operating condition to be larger than the magnetic field under the rated operating condition, which further makes the electromagnetic force under the peak operating condition higher than that under the rated operating condition.

4.2. The influence of mechanical loads on the deformation of in-wheel motor

When the in-wheel motor is in the rated operating condition, the deformation distribution of the in-wheel motor under different loads is obtained by calculating the finite element model, as shown in Fig. 5. It should be noted that in the paper, deformation is the instantaneous value of the modulus of the displacement vector. Similar to showing the reasons for the mechanical stress distribution, Fig. 5 shows the deformation distribution of the in-wheel motor at 0.06 s under the action of gravity and centrifugal force, electromagnetic force only and the combination of three loads. It can be seen from Fig. 5(a) that the maximum deformation is located on the inner edge of the rotor. Since areas with greater mechanical stress appear on the rotor, areas with greater deformation also appear on the rotor correspondingly. By comparing Fig. 5(a) and Fig. 5(b), the deformation of the outer edge of the rotor under the action of electromagnetic force is larger than that under the action of no electromagnetic force. The uneven effect of electromagnetic force also makes the stator deformation distribution no longer uniform. There are 16 large deformation areas on the stator. On the other hand, different from the action of electromagnetic force, gravity and centrifugal force act evenly on the in-wheel motor. Therefore, the deformation distribution law of Fig. 5(b) and Fig. 5(c) are the same, but the difference is the maximum deformation. Finally, under the action of the same load, since the law of deformation distribution under the peak condition is consistent with that under the rated condition, the deformation distribution under the peak condition is no longer displayed.

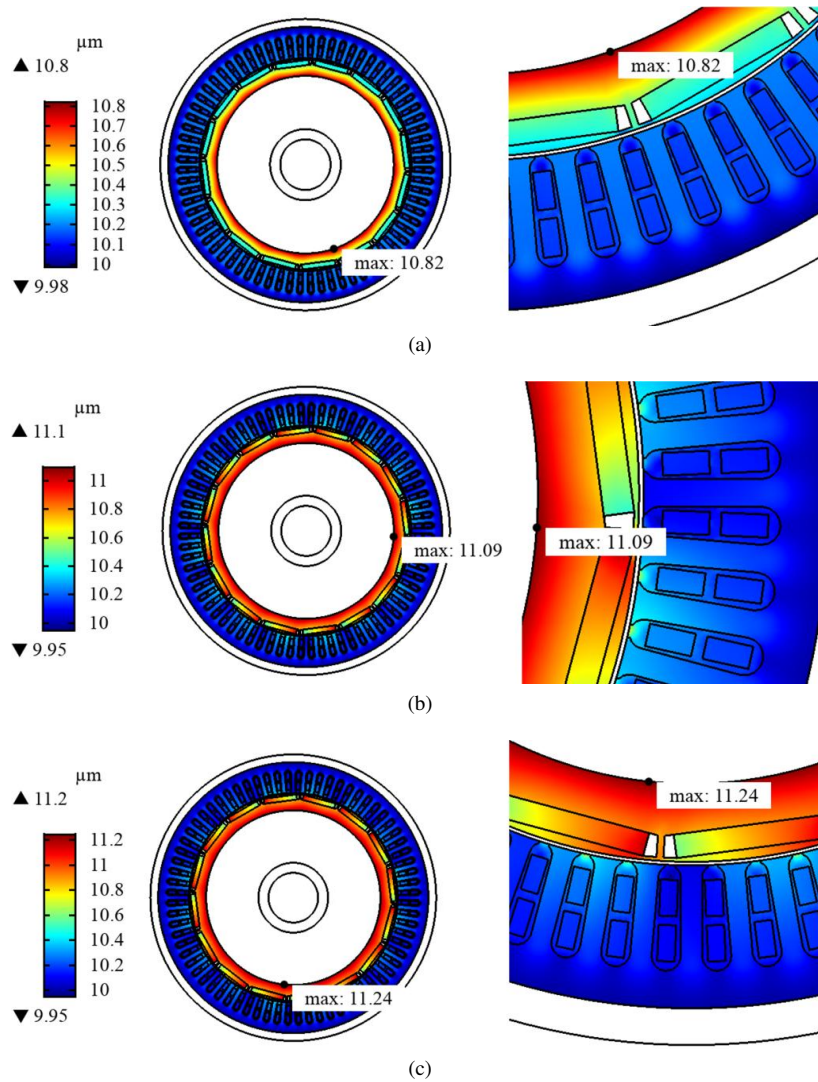


Fig. 5. Deformation distribution under rated condition: (a) gravity and centrifugal force; (b) electromagnetic force only; (c) combination of 3 loads

Table 6 shows the maximum deformation of the in-wheel motor under different operating conditions and loads. Table 7 shows the average values of deformation of the in-wheel motor under different operating conditions and loads. It can be seen from Table 6 that when the in-wheel motor is in the rated operating condition, the maximum deformation under centrifugal force only and electromagnetic force only load is 1.4% and 3.8% larger than the value under gravity only, respectively. Moreover, the maximum deformation under gravity and electromagnetic force, centrifugal force and electromagnetic force are 2.4% and 4.0% larger than the values under

Table 6. Maximum deformation of in-wheel motor (μm)

		Rated operating condition	Peak operating condition
Single load	Gravity only	10.68	10.68
	Centrifugal force only	10.83	10.86
	Electromagnetic force only	11.09	12.35
Two loads	Gravity and centrifugal force	10.82	10.85
	Gravity and electromagnetic force	11.08	12.34
	Centrifugal force and electromagnetic force	11.25	12.54
Three loads	Combination of 3 loads	11.24	12.53

Table 7. Average values of deformation of in-wheel motor (μm)

		Rated operating condition	Peak operating condition
Single load	Gravity only	10.19	10.19
	Centrifugal force only	10.23	10.24
	Electromagnetic force only	10.34	11.36
Two loads	Gravity and centrifugal force	10.23	10.24
	Gravity and electromagnetic force	10.34	11.36
	Centrifugal force and electromagnetic force	10.38	11.40
Three loads	Combination of 3 loads	10.38	11.40

centrifugal force and gravity, respectively. This is because the greater the load, the greater the deformation. Similarly, under the peak operating condition, the maximum values of deformation under centrifugal force only and electromagnetic force only loads are, respectively, 1.7% and 15.6% larger than that under the gravity only load. The maximum values of deformation under gravity and electromagnetic force, centrifugal force and electromagnetic force are 13.7% and 15.6% larger than that under centrifugal force and gravity, respectively. Obviously, it can be seen from Table 7 that for a single load, the influence of gravity only, centrifugal force only and electromagnetic force only on the average value of deformation is from small to large. For the two loads, the influence of centrifugal force and gravity, gravity and electromagnetic force, centrifugal force and electromagnetic force on the average value of deformation is from small to large. In addition, similar to the effect of load on mechanical stress, the maximum deformation under the combination of three loads is smaller than the corresponding value under the action of centrifugal force and electromagnetic force, and the average value of the deformation under

the combination of three loads is as large as the value under the action of centrifugal force and electromagnetic force.

On the other hand, under the same load (except for the case of gravity only), since the mechanical stress under the peak condition is greater than the value under the rated condition, the value of deformation under the peak condition is also greater than the value under the rated condition correspondingly.

5. Conclusions

In this paper, a 15-kW built-in permanent magnet in-wheel motor is taken as the research object. In order to consider the influence of electromagnetic force in the electromagnetic field on the structural field, the electromagnetic-structural field coupling model of the in-wheel motor is established. Based on the coupling model, the mechanical stress characteristics of the in-wheel motor under different operating conditions and mechanical loads are analyzed by the finite element method. Then, the influence laws of different mechanical loads on the mechanical stress and deformation of the in-wheel motor are obtained. The specific conclusions are as follows:

1. The results of the influence of mechanical loads on the mechanical stress of the in-wheel motor show that after the in-wheel motor is assembled, the law of mechanical stress distribution of the in-wheel motor under any load composed of gravity, electromagnetic force and centrifugal force is consistent. The rotor is the part with large mechanical stress among the parts of the in-wheel motor, and the rotor magnetic bridge is the position where the maximum mechanical stress occurs, so the rotor is easily damaged. The greater the load, the greater the mechanical stress of the in-wheel motor under the rated operating condition or peak operating condition. Therefore, the influence of gravity only, centrifugal force only and electromagnetic force only on the mechanical stress of the in-wheel motor is from small to large. At the same time, the influence of centrifugal force and gravity, gravity and electromagnetic force, centrifugal force and electromagnetic force on mechanical stress is also from small to large. Then, due to the load offset, the combined effect of three loads has a smaller effect on the mechanical stress than that happens when the centrifugal force and electromagnetic force act together. In addition, under the same load (except for the case of gravity only), the centrifugal force and electromagnetic force under the peak operating condition are greater than those under the rated operating condition, so the mechanical stress under the peak operating condition is greater than that under the rated operating condition.
2. The results of the influence of mechanical loads on the deformation of the in-wheel motor show that after the in-wheel motor is assembled, the main difference between the deformation of the in-wheel motor without electromagnetic force and with electromagnetic force lies in the deformation distribution of the rotor and stator, and the common point is that the maximum deformation is located at the inner edge of the rotor. Therefore, the rotor is easy to be damaged. Similar to the influence of loads on mechanical stress, the greater the loads, the greater the deformation. Therefore, regardless of the rated condition or peak condition, the influence of gravity only, centrifugal force only and electromagnetic force only on the deformation of the in-wheel motor is from small to large. Moreover, the influ-

ence of centrifugal force and gravity, gravity and electromagnetic force, centrifugal force and electromagnetic force on deformation is also from small to large. Then, under different loads, the combined action of centrifugal force and electromagnetic force has the greatest impact on deformation. In addition, under the same load (except for the case of gravity only), the load value under the peak operating condition is greater than that under the rated operating condition, so the deformation under the peak operating condition is greater than that under the rated operating condition.

The research work in this paper provides a theoretical basis for the subsequent reliability research of the in-wheel motor structure.

References

- [1] Chen C.Y., *Research on the vertical coupled vibration of electric vehicles driven by four-wheel hub motors*, Master Thesis, School of Automobile Engineering, Harbin Institute of Technology, Harbin (2018).
- [2] Tan D., Song F., *The advances on the study of heating and cooling issues for in-wheel-motor-driven systems*, International Journal of Electric and Hybrid Vehicles, vol. 9, no. 2, pp. 121–133 (2017), DOI: [10.1504/IJEHV.2017.085342](https://doi.org/10.1504/IJEHV.2017.085342).
- [3] Feng J., Tan D., Yuan M., *Influence of road excitation on thermal field characteristics of the water-cooled IWM*, Archives of Electrical Engineering, vol. 70, no. 3, pp. 689–704 (2021), DOI: [10.24425/aee.2021.137582](https://doi.org/10.24425/aee.2021.137582).
- [4] Qiu H.B., Zhang Y., Yang C.X., Yi R., *Performance analysis and comparison of PMSM with concentrated winding and distributed winding*, Archives of Electrical Engineering, vol. 69, no. 2, pp. 303–317 (2020), DOI: [10.24425/aee.2020.133027](https://doi.org/10.24425/aee.2020.133027).
- [5] Tian D., *Analysis of rotor dynamics characteristics of high-speed permanent magnet motors*, Master Thesis, School of Electrical Engineering, Shenyang University of Technology, Shenyang (2016).
- [6] Chaithongsuk S., Takorabet N., Rahouadj R., *Design and Construction of IPM Synchronous Motor with Magnetic and Mechanical Stress Analysis*, 2019 19th International Symposium on Electromagnetic Fields in Mechatronics, Electrical and Electronic Engineering (ISEF), pp. 1–2 (2019), DOI: [10.1109/ISEF45929.2019.9096897](https://doi.org/10.1109/ISEF45929.2019.9096897).
- [7] Lin R.Y., Sudhoff S.D., Krousgrill C., *Analytical method to compute bridge stresses in V-shape IPMs*, IET Electric Power Applications, vol. 12, no. 7, pp. 938–945 (2018), DOI: [10.1049/iet-epa.2018.0053](https://doi.org/10.1049/iet-epa.2018.0053).
- [8] Chu G.Y., Dutta R., Rahman M.F., Lovatt H., Sarlioglu B., *Analytical Calculation of Maximum Mechanical Stress on the Rotor of Interior Permanent-Magnet Synchronous Machines*, IEEE Transactions on Industry Applications, vol. 56, no. 2, pp. 1321–1331 (2020), DOI: [10.1109/TIA.2019.2960756](https://doi.org/10.1109/TIA.2019.2960756).
- [9] Chu G.Y., Dutta R., Rahman M.F., *Investigation of the Stress Concentration Factor for Estimating Maximum Mechanical Stress of Interior Permanent-Magnet Machines*, in 2018, XIII Int. Conf. on Electrical Machines, 3–6 Sept., pp. 798–804 (2018), DOI: [10.1109/ICELMACH.2018.8507225](https://doi.org/10.1109/ICELMACH.2018.8507225).
- [10] Chu G.Y., Dutta R., Lovatt H., Sarlioglu B., Rahman M.F., *Analytical Calculation of Maximum Mechanical Stress on the Rotor of the Interior Permanent-Magnet Synchronous Machine*, in 2018 IEEE Energy Conversion Congr. and Expo. (ECCE), 23–27 Sept., pp. 255–261 (2018), DOI: [10.1109/ECCE.2018.8557418](https://doi.org/10.1109/ECCE.2018.8557418).
- [11] Kleilat I., Benkara K., Friedrich G., Vivier S., Dib R., *Comparison of two Analytical Methods for Calculating the Maximum Mechanical Stress in the Rotor of High Speed Assisted Synchronous Reluctance Machines*, 2019 IEEE Energy Conversion Congress and Exposition (ECCE), pp. 1669–1674 (2019), DOI: [10.1109/TIA.2020.3040946](https://doi.org/10.1109/TIA.2020.3040946).

- [12] Jung J.W., Jeo S.M., Song D.H., *Mechanical Stress Reduction of Rotor Core of Interior Permanent Magnet Synchronous Motor*, IEEE Transactions on Magnetics, vol. 48, no. 2, pp. 911–914 (2012), DOI: [10.1109/TMAG.2011.2172582](https://doi.org/10.1109/TMAG.2011.2172582).
- [13] Huang T., Ruan J.J., Zhang Y.J., Sun M.Y., Liu H.L., Guan W.M., Hu Y.C., *Magneto-Structural Coupling Field Analysis on the End Winding of an Multi-Phase Induction Machine*, 2012 Sixth International Conference on Electromagnetic Field Problems and Applications, pp. 1–4 (2012), DOI: [10.1109/ICEF.2012.6310331](https://doi.org/10.1109/ICEF.2012.6310331).
- [14] Guo S., Guo H., Xu J.Q., *Six-phase permanent magnet fault-tolerant hub motor multi-physics comprehensive design method*, Journal of Beijing University of Aeronautics and Astronautics, vol. 45, no. 3, pp. 520–528 (2019), DOI: [10.13700/j.bh.1001-5965.2018.0360](https://doi.org/10.13700/j.bh.1001-5965.2018.0360).
- [15] Mohammed O.A., Calvert T.E., Petersen L., McConnell R., *Transient modeling of coupled magnetoelastic problems in electric machines*, IEEE Power Engineering Society Summer Meeting, vol. 1, pp. 281–287 (2002), DOI: [10.1109/PESS.2002.1043233](https://doi.org/10.1109/PESS.2002.1043233).
- [16] Ding Y., Chen Y.Y., Zhuang J.H., Li X.J., Liu F.J., *Design and Performance Investigation of Double-side Hybrid Excitation Flux-switching Machine*, 2018 IEEE International Conference on Applied Superconductivity and Electromagnetic Devices (ASEMD) IEEE, pp. 1–2 (2018), DOI: [10.1109/ASEMD.2018.8558914](https://doi.org/10.1109/ASEMD.2018.8558914).
- [17] Gao J., Zhong-Liang A.N., Chen L., Zhou T., *Rotor structure analysis of low speed and high torque permanent magnet motor*, Small and Special Electrical Machines (in Chinese), vol. 46, no. 12, pp. 4–7 (2018).
- [18] Lyskawinski W., *Comparative analysis of energy performance of squirrel cage induction motor, line-start synchronous reluctance and permanent magnet motors employing the same stator design*, Archives of Electrical Engineering, vol. 69, no. 4, pp. 967–981 (2020), DOI: [10.24425/ae.2020.134642](https://doi.org/10.24425/ae.2020.134642).
- [19] Feng X., *Research on vibration of variable frequency permanent magnet motor considering magnetostrictive effect*, Master Thesis, School of Electrical Engineering, Hebei University of Technology, Hebei (2014).
- [20] Yin Q.H., *Research on the electromagnetic-mechanical stress coupling field of permanent magnet synchronous motors*, Master Thesis, School of Electrical Engineering, North China Electric Power University, Beijing (2015).
- [21] Feng C., Li Y., Liang P., Pei Y., *Calculation of the Maximum Mechanical Stress on the Rotor of Interior Permanent-Magnet Synchronous Motors*, IEEE Transactions on Industrial Electronics, vol. 63, no. 6, pp. 3420–3432 (2016), DOI: [10.1109/TIE.2016.2524410](https://doi.org/10.1109/TIE.2016.2524410).
- [22] Roache P.J., *Error bars for CFD*, 41st Aerospace Sciences Meeting and Exhibit (2003), DOI: [10.2514/6.2003-408](https://doi.org/10.2514/6.2003-408).